

## Formation of the Microcrystalline Structure in LiNbO<sub>3</sub> Thin Films by Pulsed Light Annealing

R.N. Zhukov<sup>1</sup>, T.S. Ilina<sup>1</sup>, E.A. Skryleva<sup>1</sup>, B.R. Senatulin<sup>1</sup>, I.V. Kubasov<sup>1</sup>, D.A. Kiselev<sup>1,\*</sup>, G. Suchanec<sup>2</sup>,  
M.D. Malinkovich<sup>1</sup>, Yu.N. Parkhomenko<sup>1</sup>, A.G. Savchenko<sup>1</sup>

<sup>1</sup> National University of Science and Technology "MISiS", 4, Leninskiy Prosp., 119049 Moscow, Russian Federation

<sup>2</sup> TU Dresden, Solid State Electronics Laboratory, 01062 Dresden, Germany

(Received 11 December 2017; revised manuscript received 28 April 2018; published online 29 April 2018)

LiNbO<sub>3</sub> thin films with a thickness of 200 nm were deposited onto Al<sub>2</sub>O<sub>3</sub> substrate by RF-magnetron sputtering technique without intentional substrate heating. The results demonstrate that post-growth infrared pulsed light annealing of the amorphous LiNbO<sub>3</sub> films leads to the formation of two phases, LiNbO<sub>3</sub> and LiNb<sub>3</sub>O<sub>8</sub>. After annealing at temperatures of 700 to 800 °C, the percentage of the non-ferroelectric phase LiNb<sub>3</sub>O<sub>8</sub> was minimal. The surface composition of the films annealed at different temperatures was examined by X-ray photoelectron spectroscopy. Piezoresponse force microscopy was used to study both the vertical and the lateral polarization and to visualize the piezoelectric inactivity of LiNb<sub>3</sub>O<sub>8</sub> grains. A comparison of the results of PFM and XPS measurements revealed that there is a correlation between the fraction of the piezoelectric phase and the film composition: At an annealing temperature higher than 850 °C, the atomic ratio of lithium to niobium decreases compared to the initial value along with a decrease of the fraction of the piezoelectric phase.

**Keywords:** Lithium niobate, Li/Nb ratio, rf-magnetron sputtering, Post-growth infrared rapid annealing, Piezoresponse force microscopy, X-ray photoelectron spectroscopy.

DOI: [10.21272/jnep.10\(2\).02009](https://doi.org/10.21272/jnep.10(2).02009)

PACS numbers: 77.80.Dj, 68.55. – a, 77.55.H –

### 1. INTRODUCTION

Ferroelectric materials integrated in thin film structures have become the basis for significant improvements of functional device parameters as well as for creation of a number of innovative microelectronic devices [1]. Lithium niobate (LiNbO<sub>3</sub> or LN) is currently one of the most widely used ferroelectric materials because of its characteristic piezoelectric, electro-optical and pyroelectric properties [2]. Due to the corresponding physical effects, LiNbO<sub>3</sub> offers a large area of applications such as waveguides, surface acoustic wave devices and nonvolatile memory elements. The combination of functional properties of bulk materials and nanoscale samples allows creating structures with specified characteristics. Thin ferroelectric layers embedded into heterostructures are of interest both to fundamental research and to electronic applications. The properties of film structures strongly depend on their fabrication, electrode materials and substrate [3, 4].

One serious problem specific to LiNbO<sub>3</sub> is the precipitation of a second phase, lithium triniobates (LiNb<sub>3</sub>O<sub>8</sub>), in the crystal. This is especially pertinent when considering thin films where the crystal growth temperature is lower than the one of bulk crystals. Since the crystal structure of LiNb<sub>3</sub>O<sub>8</sub> is centrosymmetric (C<sub>2v</sub><sup>5</sup>), it possesses neither electro-optic nor ferroelectric properties. Therefore, the volume fraction of LiNb<sub>3</sub>O<sub>8</sub> should be as small as possible and that of the stoichiometric metaniobate phase, LiNbO<sub>3</sub>, should be maximized [5].

Polarization ordering and switching dynamics are among the most important issues in the physics of ferroelectrics. They should be addressed before

considering any practical applications. At present, piezoresponse force microscopy (PFM) has become a standard technique for the investigation of ferroelectric domains on the nanometer scale [6] and also for the identification of individual grains of non-ferroelectric nature in ferroelectric materials [7].

Synthesis of LiNbO<sub>3</sub> films with an optimum composition requires control of the atomic Li/Nb ratio since lithium deficiency is characteristic for the films containing the LiNb<sub>3</sub>O<sub>8</sub> phase. For these purpose we evaluate the Li/Nb ratio by means of a X-ray photoelectron spectroscopy (XPS) technique which was developed earlier for congruent lithium niobate (CLN) crystals and which is described in detail in a previous paper [8].

The aim of this work is to study the formation of the piezoelectric phase in LiNbO<sub>3</sub> thin films during their infrared (IR) pulsed light annealing and to determine the temperature range in which the fraction of the active phase of LiNbO<sub>3</sub> will be the maximum. Composition of the thin film, surface morphology and static domain structure of the LiNbO<sub>3</sub> thin films after post-deposition IR pulsed light annealing were investigated at various temperature by PFM and XPS.

### 2. EXPERIMENTAL DETAILS

Al<sub>2</sub>O<sub>3</sub> c-cut plates covered with a 150-nm-thick ITO electrode layer and a 40-nm-thick SiO<sub>2</sub> buffer layer were used as substrates. LiNbO<sub>3</sub> thin films were fabricated using a two-step method. At the first step, a 200-nm-thick amorphous layers was deposited using RF magnetron sputtering of a single-crystalline LiNbO<sub>3</sub> target in Ar/O = 60/40 atmosphere without intentionally heating the substrate. Secondly, the amorphous layers

\* [dm.kiselev@gmail.com](mailto:dm.kiselev@gmail.com)

were subjected to high temperature annealing for the formation of the  $\text{LiNbO}_3$  ferroelectric structure. IR pulsed light annealing was performed at  $600^\circ\text{C}$  to  $900^\circ\text{C}$  for 2 min in an infrared rapid heating system ULVAC VHC-P610 with a heating rate of  $5^\circ\text{C/s}$ . The final heterostructure is depicted in Fig. 1.

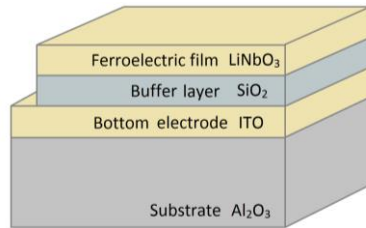


**Fig. 1** – Schematic design of the lithium niobate thin film structure fabricated on  $\text{Al}_2\text{O}_3$  substrate

The surface morphology and the static domain structure of the  $\text{LiNbO}_3$  thin films were characterized by piezoresponse force microscopy using a commercial scanning probe microscopes MFP-3D (Asylum Research, USA) with Ti/Ir coated conductive probes (Asyelec-02, Asylum Research, USA). Vertical PFM (VPFM) and lateral (LPFM) images of the samples were recorded by applying an AC voltage of  $V_{AC} = 3$  V with a frequency of 150 kHz to the cantilever.

Surface chemical composition analysis was performed by X-ray photoelectron spectroscopy. XPS measurements were performed on a VersaProbe II spectrometer (ULVAC-PHI, inc., Japan, USA) equipped with a 20 kV Ar Gas Cluster Ion Source (GCIB). Monochromatic  $\text{AlK}\alpha$  radiation ( $h\nu = 1486.6$  eV) operated at 50 W was used to excite photoemission. A focused X-ray beam diameter of  $200\ \mu\text{m}$  was scanning an analysis area of  $0.6 \times 0.3\ \text{mm}^2$ . A dual beam charge compensation system was used to provide charge neutralization at the LN film surface. High resolution spectra were recorded using a pass energy of 23.5 eV at a 0.125 eV/step for C1s, Nb3d, O1s spectra and a pass energy of 29.5 eV at 0.2 eV/step for the 50 to 70 eV region (Li1s and Nb4s spectra). The binding energies (BE) were referenced by positioning the Nb 3d5/2 peaks at a binding energy of 207.1 eV. Analysis was carried out on the as-deposited surface of the samples and after Ar GCIB irradiation. The latter was performed to remove the adsorbed contaminants.

### 3. RESULTS

The surface morphology of the  $\text{LiNbO}_3$  films annealed at various temperatures is shown in Fig. 2. The topography images revealed an increasing with increasing annealing temperature average lateral grain size of the  $\text{LiNbO}_3$  films. There is experimental evidence that surface roughness and grain size were interrelated, i.e., the average grain size was smaller at lower roughness values.

The highest grain size and roughness values were observed for  $\text{LiNbO}_3$  films annealed at  $900^\circ\text{C}$ . The temperature dependence of the average grain size and random mean square (Rms) roughness of the  $\text{LiNbO}_3$  thin films are shown in Fig. 3.

After post-deposition annealing  $\text{LiNbO}_3$  at  $900^\circ\text{C}$ , a

hexagonal crystalline structure is formed, which we

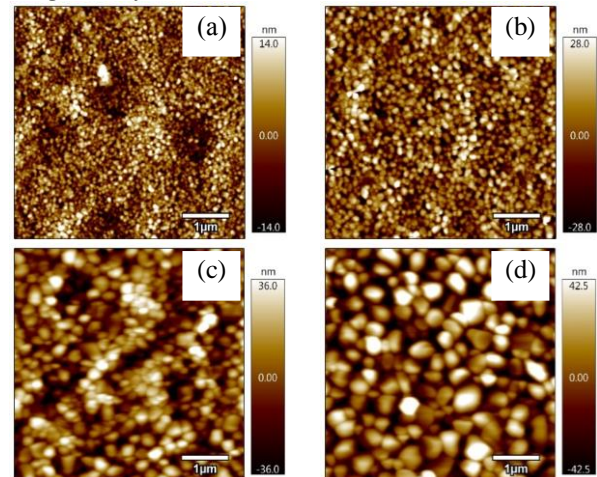


**Fig. 2** – Topography images of  $\text{LiNbO}_3/\text{SiO}_2/\text{ITO}/\text{Al}_2\text{O}_3$  heterostructures annealing at  $650^\circ\text{C}$  (a),  $750^\circ\text{C}$  (b),  $850^\circ\text{C}$  (c) and  $900^\circ\text{C}$  (d)

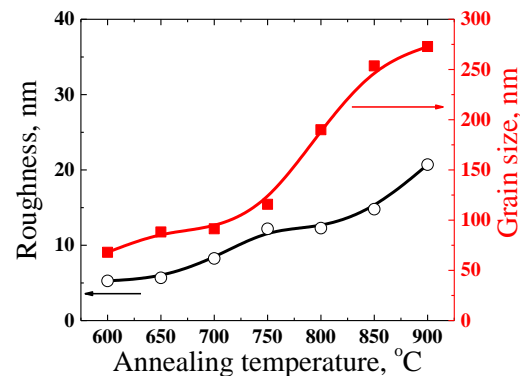


**Fig. 3** – RMS roughness and average grain size for  $\text{LiNbO}_3$  thin film as a function of annealing temperature

associate with  $\text{LiNb}_3\text{O}_8$  phase. Changes of the surface morphology with annealing temperature indicate that the phase conversion proceeds from the near-surface region of the film [5].

VPFM and LPFM images obtained simultaneously with the topography image are shown in Fig. 4. As known, the PFM modes can be used to characterize the polarization states in the ferroelectric materials [9]. The “bright” and “dark” regions on the VPFM images correspond to  $\text{LiNbO}_3$  grains with the out-of-plane polarization oriented towards the lower interface and towards the surface, respectively (Fig. 4, left column). In LPFM images (Fig. 4, right column), we visualize the piezoelectric response corresponding to the polarization direction in the plane of the film, which corresponds to the piezoelectric coefficient  $d_{15}$ . A large VPFM and LPFM signal was observed in samples  $\text{LiNbO}_3$  annealed up to  $850^\circ\text{C}$ . At the same time, the background contrast corresponds to “zero” piezoelectric response for both VPFM and LPFM images. It is attributed to the presence of non-ferroelectric particles, for example, the secondary phase  $\text{LiNb}_3\text{O}_8$ , observed previously in sol-gel derived  $\text{LiNbO}_3$  films [7].

Fig. 5 shows the piezo-histogram of a  $\text{LiNbO}_3$  film annealed at  $850^\circ\text{C}$  acquired from VPFM images in Fig. 4. Since piezo-histograms are statistical

distributions of the piezoelectric signal related to the domain configuration in a ferroelectric, the vertical tip displacement characterizing out-of-plane polarization indicates an effective longitudinal piezoelectric coefficient  $d_{33}$ . The peaks observed in this distribution curve are associated with the most probable domain configuration while the peak width is a measure of a number of domain states [10].

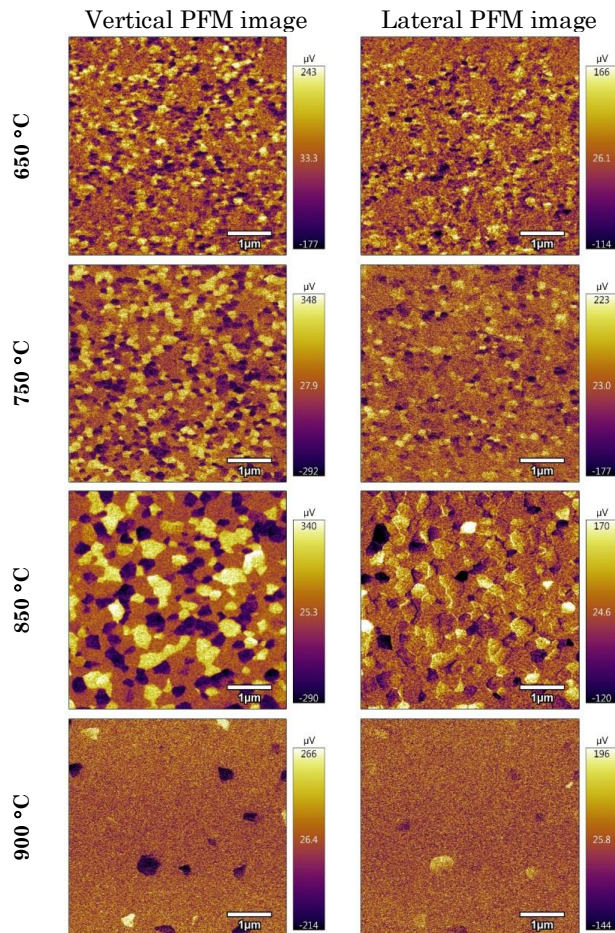


**Fig. 4** – Vertical and lateral PFM images of the  $\text{LiNbO}_3$  thin film annealed at different temperature

The piezoresponse distribution function (Fig. 5) exhibits three peaks corresponding to certain grain contrasts. This allows determination of the percentage of the grains in which the polarization vector is oriented perpendicular to the substrate plane (“up” or “down”). As it is evidenced by the distribution, part of the grains have mainly dark contrast (region #1), which corresponds to the direction of vector  $P$  from the substrate to the film surface. Region #2 corresponds to grains with zero piezoelectric response, i.e., they are piezoelectrically inactive. Grains where the polarization vector is directed from the free film surface to the substrate are marked as region #3 in the piezoelectric response distribution and the VPFM image.

The resulting area of regions 1 and 3 is  $\sim 50\%$ . Therefore, during film annealing at  $850\text{ °C}$ , the  $z$  axis is oriented parallel to the normal to surface in almost  $1/2$  of the grains. The same procedure was done for all annealed  $\text{LiNbO}_3$  thin films. Figure 6 shows the

diagram representing the ratio of piezoelectrically active grains to inactive ones ( $\text{LiNbO}_3/\text{LiNb}_3\text{O}_8$ ) calculated from VPFM histogram as a function annealing temperature.

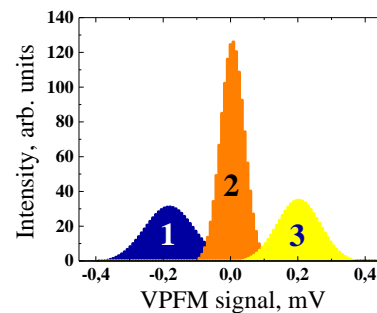


**Fig. 5** – Distribution of the vertical piezoresponse for  $\text{LiNbO}_3$  thin film annealed at  $850\text{ °C}$

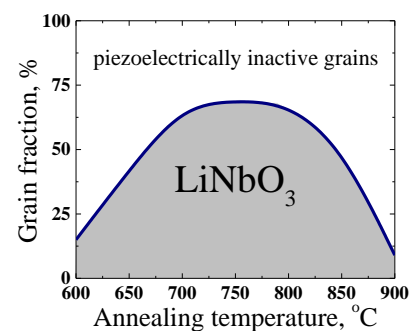


**Fig. 6** – Distribution of the grains fraction in  $\text{LiNbO}_3$  thin film annealed at various temperatures

The results demonstrate that the percentage of the non-ferroelectric phase  $\text{LiNb}_3\text{O}_8$  is minimal after annealing at temperatures of  $700$  to  $800\text{ °C}$ .

Three samples of the  $\text{LiNbO}_3$  films annealed at  $600$ ,  $750$  and  $900\text{ °C}$  were investigated by XPS. The peculiarity of the quantitative assessment of  $\text{LiNbO}_3$  is the very low intensity of the  $\text{Li}1s$  and its small width which prohibits the use of survey spectra for evaluating lithium concentration using the elemental relative sensitivity factors. To assess the lithium and niobium atomic ratio we have recorded high resolution spectrum ( $50$  to  $70\text{ eV}$ ) which contained the  $\text{Li}1s$  and  $\text{Nb}4s$  lines, measured the ratios of the integral  $\text{Li}1s$  and  $\text{Nb}4s$  intensities and calculated the atomic  $\text{Li}/\text{Nb}$  ratios by an approximate method described in detail in [8].

It is well known that the Ar-ion sputtering results in chemical damage of  $\text{LiNbO}_3$  [11]. The chemical reduction processes including the loss of oxygen and lithium and the creation of lower-valence niobium ions  $\text{Nb}^{4+}$  and  $\text{Nb}^{3+}$  are clearly visible in the  $\text{Nb}3d$  spectra as shoulder peaks at the lower binding energy side [11]. To avoid this negative phenomenon, we used an Ar gas cluster ion gun GCIB 2500Ar for surface cleaning. An acceleration voltage of  $10\text{ kV}$  at a  $2 \times 2\text{ mm}^2$  raster provides complete removal of adsorbed carbon. This is indicated in the survey spectrum after 10 min Ar cluster bombardment shown in Figure 7. Such a treatment did not result in a change of the surface chemistry as seen from the absence of shoulder peaks on the  $\text{Nb}3d$  spectrum, Fig. 7 inset.

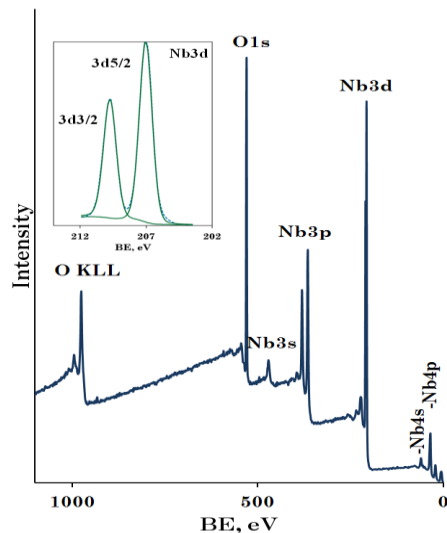


**Fig. 7** – Survey spectrum of the  $\text{LiNbO}_3$  film annealed at  $750^\circ\text{C}$  after 10 min GCIB 2500Ar irradiation. Inset shows a high resolution Nb3d spectrum

The Nb3d spin-orbit doublet of BE (3d5/2) of 207.1 eV and the energy split of 2.72 eV indicate the presence of only  $\text{Nb}^{5+}$  ions. The binding energies Li1s, Nb4s and O1s were  $55.0 \pm 0.1$  eV,  $60.2 \pm 0.1$  eV and  $530.2 \pm 0.1$  eV, respectively, the same as in the samples of CLN crystals [8].

An additional O1s peak at 532.0-532.5 eV from nonstructural oxygen with fractions of 20 to 30 % was observed on the surfaces of as-deposited samples. It disappeared after cleaning by GCIB.

The Li/Nb ratios determined from the Li1s and Nb4s spectral regions, acquired after surface cleaning, were 0.85, 0.7 and 0.5 for LN films annealed at 600, 750 and  $900^\circ\text{C}$ , respectively (Fig. 8).

These values characterize the increase of Li deficiency with temperature. Assuming the coexistence only of two phases ( $\text{LiNbO}_3$  and  $\text{LiNb}_3\text{O}_8$ ), we can estimate the  $\text{LiNbO}_3$  fraction from the atomic Li/Nb ratios 1.0 amounting for  $\text{LiNbO}_3$  and 0.33 for  $\text{LiNb}_3\text{O}_8$ , respectively. The thus obtained values were 55 % and 25 % for LN films annealed at  $750^\circ\text{C}$  and  $900^\circ\text{C}$ , correspondingly, in satisfactory agreement with the data in Figure 6. The maximum Li/Nb ratio was obtained for sample annealed at  $600^\circ\text{C}$ , but the crystal structure was not yet formed in this sample.

In general, our results show that rapid pulse light

## REFERENCES

1. J.F. Scott, *Ferroelectric Memories* (Berlin: Springer: 2000).
2. T. Volk, M. Wöhlecke, *Lithium Niobate, Defects, Photorefraction and Ferroelectric Switching* (Berlin: Springer: 2009).
3. D.A. Kiselev, R.N. Zhukov, A.S. Bykov, M.I. Voronova, K.D. Shcherbachev, M.D. Malinkovich, Yu.N. Parkhomenko, *Inorg. Mater.* **50** No 4, 419 (2014).
4. D.A. Kiselev, R.N. Zhukov, S.V. Ksenich, I.V. Kubasov, A.A. Temirov, N.G. Timushkin, A.S. Bykov, M.D. Malinkovich, V.V. Shvartsman, D.C. Lupascu, Yu.N. Parkhomenko, *J. Surf. Investig.-X-Ray* **10**, 742 (2016).
5. H. Akazawa, M. Shimada, *J. Mater. Res.* **22** No 6, 1726 (2007).
6. S.V. Kalinin, A.N. Morozovska, L.Q. Chen, B.J. Rodriguez,

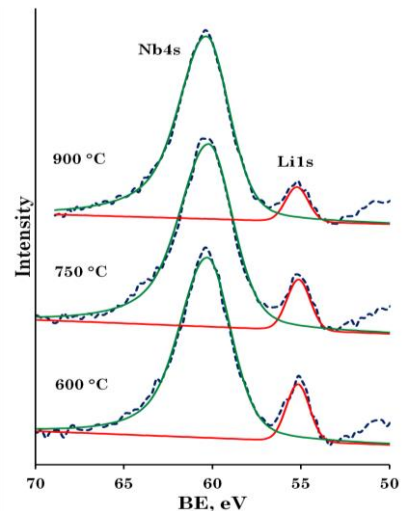


**Fig. 8** – Li1s and Nb4s spectra of the  $\text{LiNbO}_3$  films annealed at 600, 750 and  $900^\circ\text{C}$

annealing of  $\text{LiNbO}_3$  heterostructures for 1-2 minutes at temperatures of  $700^\circ\text{C}$  to  $800^\circ\text{C}$  leads to similar results as long-term furnace annealing for several hours reported in Ref. [5].

## 4. CONCLUSIONS

In summary,  $\text{LiNbO}_3$  ferroelectric films were grown onto  $\text{Al}_2\text{O}_3$  substrate by RF-magnetron sputtering. A post-growth IR pulsed light annealing of the as-grown amorphous  $\text{LiNbO}_3$  films in wide temperature range of  $600$ - $900^\circ\text{C}$  leads to the formation of two phases,  $\text{LiNbO}_3$  and  $\text{LiNb}_3\text{O}_8$ . From PFM and XPS data, we obtained that the percentage of the non-ferroelectric phase  $\text{LiNb}_3\text{O}_8$  is minimal after annealing at temperatures of  $700$  to  $800^\circ\text{C}$ .

## ACKNOWLEDGEMENT

The studies were performed on the equipment of Center for Shared Use “Materials Science and Metallurgy” at the National University of Science and Technology “MISIS”. The research was financially supported by the Ministry of Education and Science of the Russian Federation (Federal Targeted Programme for Research and Development in Priority Areas of Development of the Russian Scientific and Technological Complex for 2014-2020, Project ID RFMEFI58716X0035).

*Rep. Prog. Phys.* **73** No 5, 056502 (2010).

7. F. Johann, T. Jungk, S. Lisinski, A. Hoffmann, L. Ratke, E. Soergel, *Appl. Phys. Lett.* **95**, 202901 (2009).
8. E.A. Skryleva, I.V. Kubasov, Ph.V. Kiryukhantsev-Korneev, B.R. Senatulin, R.N. Zhukov, K.V. Zakutailov, M.D. Malinkovich, Yu.N. Parkhomenko, *Appl. Surf. Sci.* **389**, 387 (2016).
9. A. Wu, P.M. Vilarinho, V.V. Shvartsman, G. Suchaneck, A.L. Kholkin, *Nanotechnology* **16**, 2587 (2005).
10. M. Melo, E.B. Araújo, V.V. Shvartsman, V.Ya. Shur, A.L. Kholkin, *J. Appl. Phys.* **120**, 054101 (2016).
11. X. Bai, Y. Shuai, Ch. Gong, Ch. Wu, W. Luo, R. Böttger, Sh. Zhou, W. Zhang, *Appl. Surf. Sci.* **434**, 669 (2018)